DOI:10.1111/j.1600-0625.2010.01128.x
www.blackwellpublishing.com/EXD

Original Article

Protective effects of platinum nanoparticles against UV-light-induced epidermal inflammation

Yoko Yoshihisa[1], Ayumi Honda[1,2], Qing-Li Zhao[3], Teruhiko Makino[1], Riichiro Abe[2], Kotaro Matsui[1], Hiroshi Shimizu[2], Yusei Miyamoto[4], Takashi Kondo[3] and Tadamichi Shimizu[1]

[1]Department of Dermatology, Graduate School of Medicine and Pharmaceutical Sciences, University of Toyama, Sugitani, Toyama, Japan;
[2]Department of Dermatology, Graduate School of Medicine, Hokkaido University, Sapporo, Japan;
[3]Department of Radiological Sciences, Graduate School of Medicine and Pharmaceutical Sciences, University of Toyama, Sugitani, Toyama, Japan;
[4]Department of Integrated Biosciences, Graduate School of Frontier Sciences, University of Tokyo, Chiba, Japan
Correspondence: Tadamichi Shimizu, Department of Dermatology, Graduate School of Medicine and Pharmaceutical Sciences, University of Toyama, Sugitani, Toyama, Japan, Tel.: +81-76-434-7305, Fax: +81-76-434-5028, e-mail: shimizut@med.u-toyama.ac.jp

Accepted for publication 21 April 2010

Abstract: Intracellular reactive oxygen species (ROS) and apoptosis play important roles in the ultraviolet (UV)-induced inflammatory responses in the skin. Metal nanoparticles have been developed to increase the catalytic activity of metals, which is because of the large surface area of smaller particles. Platinum nanoparticles (nano-Pt) protected by poly acrylic acid were manufactured by reduction with ethanol. A marked increase in ROS production was observed in UV-treated HaCaT keratinocytes cell lines, while a decrease in ROS production was observed in nano-Pt-treated cells. Pretreatment of the cells with nano-Pt also caused a significant inhibition of UVB- and UVC-induced apoptosis. Furthermore, we found that mice treated with nano-Pt gel prior to UV irradiation showed significant inhibition of UVB-induced inflammation and UVA-induced photoallergy compared to UV-irradiated control mice. These results suggest that nano-Pt effectively protects against UV-induced inflammation by decreasing ROS production and inhibiting apoptosis in keratinocytes.

Key words: apoptosis – platinum nanoparticles – reactive oxygen species – skin – ultraviolet

Please cite this paper as: Protective effects of platinum nanoparticles against UV-light-induced epidermal inflammation. Experimental Dermatology 2010; **19**: 1000–1006.

Introduction

Skin is a major target for toxic insult by a broad spectrum of ultraviolet (UV) radiation that is capable of altering its structure and function. Photodamaged skin exhibits wrinkles, pigmented spots, dryness, and tumors. UV radiation has been reported to generate reactive oxygen species (ROS), such as singlet oxygen, superoxide radicals, hydroxyl radicals, and hydrogen peroxide, in a variety of cells (1), and intracellular ROS are thought to play an important role in UV-induced inflammatory responses in the skin. Both short-wavelength UVC (200–280 nm) and UVB (280–320 nm) as well as long-wavelength UVA (320–400 nm) produce ROS, which can lead to cell damage when the balance between the prooxidant stimuli and cellular antioxidant defenses is impaired (2,3).

The skin has a complex defense system of enzymatic and non-enzymatic components to counter the adverse biological effects of ROS. As the first defense, ROS are reduced by antioxidant enzymes, such as superoxide dismutase (SOD), catalase, and glutathione peroxidase, as well as endogenous and exogenous small molecules, including glutathione and vitamins C and E. When biomolecules are oxidized, they are repaired or replaced by biological protective systems. Nevertheless, biomolecules are gradually irreversibly oxidized, and accumulation of these biomolecules over time impairs biological functions, eventually leading to ageing and age-related diseases (4,5). Sunscreen use is a widely accepted method of primary prevention against skin cancer, sunburn, and photoageing. In fact, antioxidant compounds used in these products seem to function as protective substances against UV-induced ROS in the skin. Topical antioxidants, such as the flavonoid quercetin, have been reported to diminish UV radiation–mediated oxidative damage to the skin (6,7). Ascorbic acid (AA), which is the

Abbreviations: AA, ascorbic acid; IL, interleukin; MIF, macrophage migration inhibitory factor; MMP, mitochondrial membrane potential; nano-Pt, platinum nanoparticles; ROS, reactive oxygen species; TNF, tumor necrosis factor; UV, ultraviolet; LFLX, lomefloxacin hydrochloride.

most abundant antioxidant in the dermis, has exhibited a protective effect against oxidative stress.

Metal nanoparticles have been developed to increase the catalytic activity of metals because of the large surface area of smaller particles. Some noble metal nanoparticles are reducing catalysts that may be useful as antioxidants acting to reduce ROS in a living body. Nanotechnology is of interest because of the wide application of nanoparticles not only in material science and engineering but also in medical science and clinical use. Platinum nanoparticles (nano-Pt) protected by polyacrylic acid were recently manufactured by reduction with ethanol for 2 h (8). Nano-Pt are known to function as reductive catalysts; thus, they may be used as antioxidants to reduce ROS in living organisms. In fact, nano-Pt have the ability to scavenge O_2^- and H_2O_2, indicating that nano-Pt can act as a SOD/catalase mimetic (8). However, only a few studies have reported the antioxidant effects of nano-Pt in living organisms.

To elucidate the possible role of nano-Pt in UV-induced skin damage, we examined their protective effect on UV-induced ROS production and apoptosis using cultured keratinocytes. We also investigated the role of topically applied nano-Pt against UV-induced skin damage in mice.

Materials and methods

Reagents

Anti-Bcl-X_L monoclonal antibody (mAb), anti-Bax polyclonal antibody (pAb), anti-caspase-3 pAb, and anti-β-actin Ab were obtained from Santa Cruz Biotechnology, Inc.(Santa Cruz, CA, USA); nano-Pt were prepared as described previously (8). Nano-Pt gel was formulated by mixing 0.02% nano-Pt in water (corresponding to approximately 1 mM) with water and carboxyvinyl polymer (WAKO, Tokyo, Japan) (nano-Pt:water:carboxyvinyl polymer = 1:8.8:0.2) to yield a 0.002% w/w gel. Other reagents were of analytical grade.

Cell culture

HaCaT cells, an immortalized, non-tumorigenic human keratinocyte cell line (9), were maintained in DMEM (Invitrogen, Carlsbad, CA, USA) supplemented with 10% foetal bovine serum and 1% antibiotics at standard cell culture conditions (37°C, 5% CO_2 in a humidified incubator).

Mice

Eight-week-old male Balb/c mice were purchased from Japan Clea (Shizuoka, Japan). These mice were maintained under specific pathogen-free conditions. All experiments involving mice were performed in accordance with the guidelines for the care and use of laboratory animals at the Hokkaido University Graduate School of Medicine and University of Toyama.

UV irradiation

The UVA irradiation source was a FL20S/BLB fluorescent lamp (Clinical Supply, Tokyo, Japan) that emitted an energy spectrum with high fluency in the UVA region (300–430 nm), with a peak at 352 nm. A 6-mm-thick glass plate was used to block UVB emissions. The UVB light source was a FL20SE30 (Clinical Supply Co., Tokyo, Japan) fluorescent lamp that emitted 1.0 mW/cm^2 of UV radiation between 280 and 370 nm (peak 305 nm) at a distance of 25 cm, as measured by a UV radiometer (Torex Co., Tokyo, Japan). The UVC light source was a 615T8 (Sanyo Denki., Tokyo, Japan) fluorescent lamp that emitted 15 W of UV radiation between 190 and 280 nm (peak 254 nm) at a distance of 25 cm, as measured by a UV radiometer (Funakoshi Co., Tokyo, Japan).

Assessment of intracellular ROS

Intracellular ROS were measured using hydroethidine (HE) (Molecular Probes, Eugene, OR, USA) to detect intracellular superoxide (O_2^-) (10). HE is oxidized by O_2^- within the cells to produce ethidium bromide, which fluoresces when it intercalates into DNA. After 30 min of incubation following different treatments, the cells were stained with either 2 μM HE and incubated for 15 min at 37°C in darkness. Fluorescence emission of the resulting dyes was then analysed by flow cytometry.

Assay of DNA fragmentation

For the detection of apoptosis, the percentage of DNA fragmentation was assessed 24 h post treatment using the method of Sellins and Cohen (11) with minor modifications. In brief, approximately 3×10^6 cells were lysed using 200 μl of lysis buffer and centrifuged at 13 000 g for 10 min. Subsequently, DNA from each sample in the supernatant, and pellet was precipitated in 12.5% trichloroacetic acid (TCA) at 4°C overnight and quantified using the diphenylamine reagent after hydrolysis in 5% TCA at 90°C for 20 min. The percentage of fragmented DNA for each sample was calculated as the amount of DNA in the supernatant divided by the total DNA for that sample (supernatant plus pellet).

Assessment of early apoptosis and secondary necrosis

To determine the amount of early apoptosis and secondary necrosis, cells were collected 24 h post treatment and simultaneously stained with propidium iodide- and fluorescein isothiocyanate (FITC)-labelled annexin V, according to the instructions of the annexin V-FITC kit (Immunotech, Marseille, France) and finally, analysed with a flow cytometer (Beckman-Coulter EPICS XLTM) (12).

Measurement of mitochondrial membrane potential (MMP)

To measure changes in MMP, control cells and cells treated with nano-Pt (100 μM), HT, and a combination of both were collected at 6 h post treatment. The cells were then stained with 10 nM tetramethylrhodamine methyl ester (TMRM) (Molecular Probes, Eugene, OR) for 15 min at 37°C in phosphate-buffered saline (PBS) containing 1% FBS. The fluorescence of TMRM was analysed using flow cytometry (excitation at 488 nm; emission at 575 nm) (13).

Assay of UVB-induced inflammation and apoptosis *in vivo*

The mice were placed in individual compartments of specially designed cages, and their ears were exposed once to 350 mJ/cm^2 of UVB radiation. One group was treated with nano-Pt ointment on the earlobes (0.3 g on each earlobe) 24 h and immediately (two times) prior to UVB irradiation, while the other group was treated with carboxyvinyl polymer gel alone. The thickness of each ear was measured using a spring-loaded micrometre (Mitutoyo, Tokyo, Japan) to determine the baseline thickness. Ear swelling was calculated as the difference in ear thickness between the 24 h and the baseline values (14).

TUNEL assay

After 24 h, 350 mJ/cm^2 of UVB-irradiated mouse skin was obtained and analysed by TUNEL assay according to the manufacturer's instructions (R&D Systems). For statistical analysis, apoptotic cells were counted by light microscopy (100×) and expressed as the mean number (±SD) of apoptotic cells per section. Five random fields per section (one section per mouse, five mice per group) were analysed.

Assay of fluoroquinolone photoallergy

Fluoroquinolone photoallergy is inducible in Balb/c mice when they are sensitized by systemic administration of lomefloxacin hydrochloride (LFLX) (2 mg/0.2 ml, i.p.) followed by 12 J/cm^2 UVA irradiation of the shaved abdomen and challenged with systemic quinolone and UVA exposure of the earlobes (20 J/cm^2) (15). One group was treated with nano-Pt ointment on the earlobes (0.3 g on each earlobe) 24 h before and immediately (two times) prior to UVA challenge, while the other group was treated with carboxyvinyl polymer gel alone. Ear thickness was measured using an engineer's micrometre 6–10 days after the challenge and compared with ear thickness before the challenge.

Histological observation

Ears were fixed in 10% PBS-buffered formalin, and paraffin sections were stained with haematoxylin and eosin and examined by light microscopy to assess histological changes.

Northern blot analysis

Total cellular RNA was isolated from epidermis using the Isogen extraction kit according to the manufacturer's instructions. The epidermis was separated from the dermis by incubation in 0.5% dispase in RPMI-1640 at 37°C for 1 h. RNA was quantified spectrophotometrically, and equal amounts of RNA (10 μg) from samples were loaded on a formaldehyde-agarose gel. The gel was stained with ethidium bromide to visualize the RNA strands, and the RNA was transferred onto a nylon membrane. Fragments obtained by restriction enzyme treatments for tumor necrosis factor (TNF)-α, interleukin (IL)-1β, macrophage migration inhibitory factor (MIF), and GAPDH were labelled with [α-^{32}P]dCTP using a DNA random primer labelling kit. Hybridization was performed using the mouse MIF cDNA probe as described previously. The cDNA probes for TNF-α were 5′-TCTCATCAGTTCTATGGCCC-3′ (forward) and 5′-GGGAGTAGACAAGGTACAAC-3′ (reverse) and for IL-1β were 5′-CCCATACTTTAGGAAGACACGGATT-3′ (forward) and 5′-TCATGGGATGATGATGATAACCTGCT-3′ (reverse). The membrane was washed twice with 2× SSC (16.7 mM NaCl, 16.7 mM sodium citrate) at 22°C for 5 min, twice with 0.2× SSC containing 0.1% SDS at 65°C for 15 min, and twice with 2× SSC at 22°C for 20 min prior to autoradiography. The density of cytokine bands was normalized by the GAPDH intensities.

Western blot analysis

Cells were collected and washed with cold PBS. They were lysed at a density of 1 × 10^6 cells/50 μl of RIPA buffer (1 M Tris-HCl, 5 M NaCl, 1% Nonidet P-40 (v/v), 1% sodium deoxycholate, 0.05% SDS, 1 mM phenylmethyl sulfonyl fluoride) for 20 min. Following brief sonification, the lysates were centrifuged at 12 000 ***g*** for 10 min at 4°C, and the protein content in the supernatant was measured using the Bio-Rad protein assay kit (Bio-Rad, Hercules, CA, USA). Protein lysates were denatured at 96°C for 5 min after mixing with 5 μl SDS-loading buffer, applied on an SDS-polyacrylamide gel for electrophoresis, and transferred to nitrocellulose membranes. Western blot analysis was performed to detect Bcl-X_L, Bax, and caspase-3 expression using specific antibodies. Band signals were visualized on X-ray film using chemiluminescence ECL detection reagents (Amersham Biosciences, Buckinghamshire, UK) (16). Band density was quantified by a BIO-ID image analyzer, and the relative amounts of proteins associated with specific antibodies were normalized according to the intensities of β-actin.

Measurement of intracellular Pt content

The cells (1 × 10^7 cells) treated for 24 h with or without nano-Pt (100 μM) were collected by centrifugation, and the pellets were frozen. After thawing, each sample was placed in a glass vessel and reconstituted in nitric acid and hydrogen

peroxide (1:1). The solutions were evaporated to dryness on a hot plate and then, the residues were dissolved in dilute aqua regia (4 vol. %). Quantitative analysis of Pt for each solution was performed using inductively coupled plasma mass spectrometry (Model ELAN DRC II: Perkin Elmer SCIEX; Perkin Elmer Inc., Franklin, MA, USA).

Statistical analysis

Differences between the various treatments were statistically analysed using Student's *t*-test. For comparisons of multiple groups, one-way ANOVA was applied to the data. Furthermore, P values <0.05 were considered statistically significant. Data in the figures are shown as the mean ± SD of several experiments.

Results

Effects of nano-Pt on ROS production

We examined the effects of nano-Pt on UV-induced ROS production in keratinocytes. HaCaT cells were UV-treated with or without nano-Pt at different concentrations for 24 h, and flow cytometry with HE staining was used to detect ROS production in these cells. A marked increase in the production of O_2^- was observed 30 min after UV treatment in the cells. Nano-Pt at 100 μM concentration significantly inhibited each UV-induced O_2^- ($P \leq 0.001$) (Fig. S1). Therefore, we used nano-Pt at 100 μM concentration for next series of experiments. The percentage of cells producing O_2^- increased after UVA, UVB, and UVC irradiation dose dependently. Nano-Pt significantly inhibited UV-induced O_2^- [UVA 20 J/cm^2: 36.2 ± 2.1% ($P \leq 0.001$), UVB 60 mJ/cm^2: 26.0 ± 1.6% ($P < 0.05$), and UVC 60 mJ/cm^2: 42.7 ± 10.8% ($P \leq 0.001$)] (Fig. S1).

Effects of nano-Pt on UV-induced apoptosis

To investigate whether nano-Pt have the ability to protect against UV-induced apoptosis, HaCaT cells were UV-treated with or without nano-Pt (100 μM) for 24 h, and the effects were determined by evaluating DNA fragmentation in the cells. When these cells were pretreated with nano-Pt for 24 h, UVB- and UVC-induced apoptosis was significantly inhibited. On the other hand, nano-Pt had little effect on UVA-induced apoptosis, nano-Pt had only effective on 5 J/cm^2 UVA irradiation (Fig. 1). Annexin V-FITC-propidium iodide staining was used as a parameter for detecting apoptotic cell death, and the number of early apoptotic cells increased after UVB (20 and 40 mJ/cm^2) and UVC (20 and 40 mJ/cm^2) irradiation. Treatment with nano-Pt (100 μM) before UVB and UVC irradiation reduced the number of early apoptotic cells compared to UVB or UVC alone (Fig. 2). On the other hand, nano-Pt had no effect on UV-induced secondary necrosis.

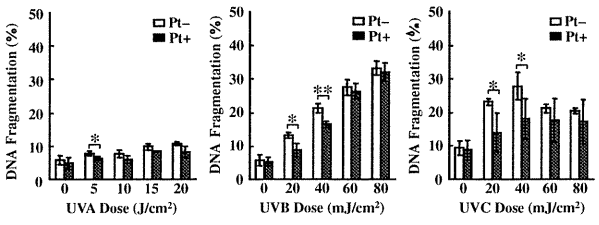

Figure 1. Effects of nano-Pt on ultraviolet-induced apoptosis. Cells were treated with UVA (5–20 J/cm^2), UVB (20–80 mJ/cm^2), and UVC (20–80 mJ/cm^2) with or without nano-Pt (100 μM) for 24 h. DNA fragmentation assay was performed after 24-h incubation at 37°C. Data are presented as mean ± SD (n = 5). *P < 0.05, **$P \leq$ 0.01. Data shown are representative of three independent experiments.

Expression of apoptosis-related proteins

Next, we evaluated changes in apoptotic marker proteins as a result of UV irradiation and exposure to nano-Pt (100 μM). The relative density of Bax, Bcl-X_L, and procaspase-3 to β-actin, calculated by integrating the density values of these three proteins, was similar in all the treated groups. The relative density of Bax to β-actin was 3.2 and 2.1 in samples irradiated with UVB and UVC, respectively. Nano-Pt decreased UVB- and UVC-induced Bax expression (UVB, 1.5; UVC, 1.7). The relative density of Bcl-X_L to β-actin was 0.08 in the UVB-irradiated samples. Furthermore, nano-Pt resulted in an increase in the UVB-induced Bcl-X_L expression (0.1) but did not alter the UVC-induced Bcl-X_L expression level. However, UVA irradiation did not alter Bax and Bcl-X_L expression levels. Expression of procaspase-3 decreased because of UVB and UVC irradiation and increased because of nano-Pt (Fig. 3). On the other hand, nano-Pt had no effect on Bax, Bcl-X_L, and procaspase-3 expression by UVA irradiation.

Effects of nano-Pt on Fas and the mitochondrial pathway

To examine the effects of nano-Pt on Fas externalization, cells were treated with or without 100 μM of nano-Pt for

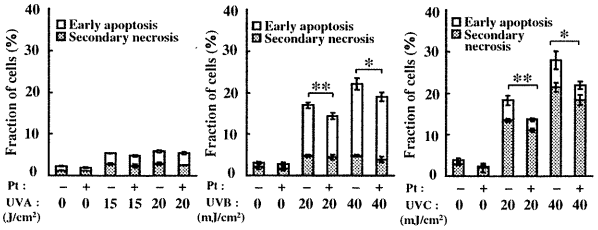

Figure 2. Effects of nano-Pt on ultraviolet (UV)-induced early apoptosis and secondary necrosis. Cells were treated with UVA, UVB, and UVC with or without nano-Pt (100 μM) for 24 h. Percentages of early apoptosis and secondary necrosis were analysed 24 h after UV treatment by flow cytometry. Data are presented as mean ± SD (n = 5). *$P \leq$ 0.05, **$P \leq$ 0.01. Data shown are representative of three independent experiments.

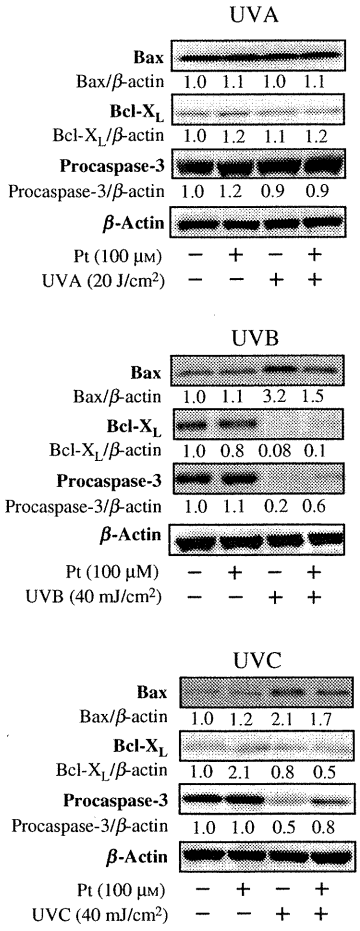

Figure 3. Ultraviolet-induced expression of apoptosis-related proteins. Immunoblot analysis of various apoptosis-related proteins in cells exposed to UVA, UVB, and UVC with or without nano-Pt (100 μM). Cell extracts were subjected to 5–20% SDS-PAGE and immunoblotted with antibodies against cleaved Bax, Bcl-X_L, caspase-3, and β-actin. Densitometry data, standardized by β-actin are presented below the band. Data shown are representative of three independent experiments.

24 h. Nano-Pt had no effect on UV-induced Fas production. Next, the effects of nano-Pt on the loss of mitochondrial membrane potential ($\Delta\Psi m$), which is an endpoint of apoptosis, were examined in HaCaT cells exposed to UV. Significant decrease in the loss of $\Delta\Psi m$ was observed (14.6 ± 3.1%; $P < 0.01$) when compared to UVB irradiation alone (Table 1).

Measurement of intracellular Pt content

When the intracellular content of Pt in samples was measured by inductively coupled plasma mass spectrometry, the values were 200 ng for treated cells and ≤0.05 ng for untreated control cells. Thus, intracellular incorporation of Pt was observed.

Table 1. Effects of nano-Pt endpoints of apoptosis

	Fas (%)	MMP (%)
Control	5.0 ± 0.1	5.0 ± 0.1
Pt + (100 μM)	5.1 ± 0.2	4.6 ± 0.4
UVA (20 J/cm^2)	21.6 ± 0.9	25.8 ± 1.6
Pt + UVA (20 J/cm^2)	20.7 ± 0.5	23.3 ± 2.0
UVB (40 mJ/cm^2)	15.6 ± 2.6	19.8 ± 1.2
Pt + UVB (40 mJ/cm^2)	13.2 ± 1.3	14.6 ± 3.1*
UVC (40 mJ/cm^2)	12.5 ± 2.8	9.6 ± 0.7
Pt + UVC (40 mJ/cm^2)	10.3 ± 1.7	9.2 ± 0.8

Cells were ultraviolet (UV) treated with or without nano-Pt (100 μM) for 24 h. The percentages of fraction of Fas positive cells are analyzed after UV treatment by flow cytometry using anti-Fas FITC antibody staining, and the percentages of loss of MMP are analyzed after UV treatment by flow cytometry using TMRM staining. The results are presented as the mean ± SD ($n = 5$).
*$P < 0.01$ vs UVB (40 mJ/cm^2).
MMP, mitochondrial membrane potential.

Effects of nano-Pt on UVB-mediated inflammation and apoptosis in mice

To present these results in an *in vivo* context, we analysed the role of nano-Pt ointment in UV-induced skin inflammation in mice. We assessed UVB irradiation–induced inflammation on the earlobes of mice. Twenty-four hours after 350 mJ/cm^2 UVB irradiation, the ear swelling in mice pretreated with nano-Pt gel was significantly decreased compared to that in UVB-irradiated control mice treated with carboxyvinyl gel polymer ($P < 0.01$) (Fig. S2). Immunochemical analysis demonstrated that a large number of TUNEL-positive cells were detected in the control mice after UVB irradiation, whereas few TUNEL-positive cells were detected in nano-Pt-treated mice ($P < 0.01$) (Fig. 5b,c). Thus, the nano-Pt-treated mice demonstrated a significantly smaller number of apoptotic cells than the control mice.

Effects of nano-Pt on photoallergy to LFLX plus UVA irradiation in mice

Subsequent studies were aimed to assess whether nano-Pt inhibit UVA-induced photoallergy. Fluoroquinolone photoallergy can be induced in Balb/c mice by sensitizing them by systemic administration of LFLX (2 mg/0.2 ml, i.p.), followed by 12 J/cm^2 UVA irradiation of the shaved abdomen, and posing a challenge using systemic quinolone and UVA exposure of the earlobes (20 J/cm^2). Significant ear swelling was observed in the positive control mice treated with carboxyvinyl polymer gel, but this response was inhibited in the earlobes of mice treated with nano-Pt gel prior to UVA irradiation ($P \leq 0.001$) (Fig. S3). Histological evaluation demonstrated that nano-Pt-treated mice had reduced cutaneous oedema, leucocyte infiltration, and hyperplasia even

on day 5 (Fig. S3). Northern blot analysis of the proinflammatory cytokine mRNA levels in the earlobes on day 5 showed decreased TNF-α, IL-1,β, and MIF expression in the nano-Pt-treated skin when compared to the positive control mouse skin (Fig. S3).

Discussion

UV irradiation of the skin results in a variety of injuries involving inflammatory and repair reactions, free radical reactions, and apoptosis. These injuries include immediate consequences, such as erythema and pigmentation, as well as delayed changes, such as cellular DNA mutations, hyperplasia, and carcinogenesis (17). ROS produced by UV radiation have the potential to damage critical cellular components, such as DNA, proteins, and lipids, eventually causing physical and chemical damage to skin tissues that may lead to cell death. To counteract oxidative injury, the skin is equipped with a network of enzymatic and non-enzymatic antioxidant systems, such as tocopherols and ascorbate polyphenols (18). This study demonstrated that treatment with nano-Pt reduced production of O_2^- in HaCaT cells before UV irradiation. Metal nanoparticles have been developed to increase the catalytic activity of metals because of the large surface area of smaller particles. Because nano-sized particles can reflect shorter wavelengths (UV light) (19), nanoparticles in the form of TiO_2 and ZnO have been used in sunscreen preparations to protect human skin physically. However, nano-Pt have been expected to protect human skin both physically and chemically owing to their SOD/catalase mimetic activity (8). Furthermore, compared to other metal nanoparticles, nano-Pt function as high reductive catalysts and may thus act as antioxidants to reduce ROS (8). Recently, Onizawa et al. demonstrated that treatment of alveolar-like A549 cells with nano-Pt inhibited cell death after exposure to a cigarette smoke extract. These results suggest that nano-Pt act as antioxidants that inhibit pulmonary inflammation induced by acute cigarette smoking (20). Furthermore, it has been demonstrated that nano-Pt prolonged the lifespan of worms, regardless of thermotolerance or dietary restriction (21). In this context, we suggest that nano-Pt are effective in reducing ROS production in UV-irradiated keratinocytes. Therefore, nano-Pt may have interesting anti-skin ageing properties.

Because DNA fragmentation, an endpoint of apoptosis, has been observed in human keratinocytes and HaCaT cells under certain conditions (22–24), we aimed at checking apoptosis-induction profile following different treatments using DNA fragmentation assay. The results revealed the occurrence of significant DNA fragmentation in HaCaT cells after UV irradiation. In this study, HaCaT cells irradiated with UVA, UVB, and UVC at different wavelengths demonstrated dose-dependent apoptosis following UVB and UVC exposure only, whereas no significant apoptosis was detected after UVA irradiation. Although UVA was shown to elevate intracellular superoxide production, it also induced delayed and sustained activation of extracellular signal-regulated kinase (ERK), which is apoptotic suppressor (25), and upregulation of the antiapoptotic protein Bcl-X_L by p38 MAPK activation (26). These simultaneous and opposing effects resulted in alleviation of the apoptotic stimulus. When HaCaT cells were irradiated with UVB and UVC in the presence of nano-Pt, UV-induced apoptosis was partially suppressed at 20 and 40 mJ/cm^2 in both cases. Because nano-Pt significantly attenuated superoxide formation in cells treated with UVA, UVB, and UVC but had no effect on peroxide formation, we concluded that superoxide plays an essential role in UVB- and UVC-induced apoptosis. It has been demonstrated that ROS increases the expression of cell surface Fas in human airway epithelial cells by promoting cytoplasmic transport of Fas (27). Thus, a putative mechanism of UVB- and UVC-induced apoptosis in HaCaT cells may involve accelerated recruitment of Fas on the cell membrane in response to elevated intracellular ROS, particularly superoxide, produced by UV irradiation. The apoptotic signal mediated by Fas guides the mitochondrial pathway and activation of caspase-3.

Similarly, our results demonstrated a significant increase in Fas expression and decrease in MMP in all UV-treated cells. On the other hand, a tendency for reduction in Fas expression and restoration of the decreased MMP content in the presence of nano-Pt was observed but was without statistical significance, except in case of UVB. When the Bcl-2 family proteins were measured, increased expression of the proapoptotic protein Bax and decreased expression of the antiapoptotic protein Bcl-X_L by UVB and UVC were reported. These effects were the opposite in the presence of nano-Pt. Furthermore, our data revealed caspase-3 activation by UV irradiation and its inhibition in the presence of nano-Pt. Therefore, the involvement of the mitochondrial caspase pathway and its modulation by intracellular superoxide in UV-induced apoptosis in HaCaT cells was confirmed. With respect to the localization of nanoparticles, Kiss et al. reported that TiO_2 nanoparticles cannot be uptaken by HaCaT cells (28). However, our results demonstrated the intracellular uptake of nano-Pt by HaCaT cells. Thus, we suggest that nano-Pt exerts protective effects because of their intracellular ROS scavenging activity.

The skin is continuously exposed to sunlight and environmental oxidizing pollutants; it is the preferred target of oxidative stress (29). Evidence suggests that signs of skin ageing, such as wrinkling, sagging, and actinic lentigines, may be associated with the cumulative oxidative damage incurred throughout our life. This study also demonstrates that nano-Pt gel applied topically on mouse skin protects against UVB-induced inflammation. Furthermore, we

demonstrated that nano-Pt have an antiapoptotic effect against UVB irradiation *in vivo*. UVB affects skin by inducing immunosuppression, premature skin ageing, inflammation, and cell death. Recent findings from our *in vivo* and *in vitro* observations suggest that nano-Pt can scavenge and inhibit inflammatory responses and apoptosis in the skin, which is caused by UVB exposure. Moreover, we found that nano-Pt gel was useful in mice with fluoroquinolone photoallergy. Fluoroquinolone photoallergy in mice is a model of photosensitivity dermatitis induced by UVA irradiation (30). Our results demonstrated that UVA-induced inflammation was clinically and histologically reduced by nano-Pt gel. Furthermore, proinflammatory cytokine levels in skin tissues decreased by nano-Pt treatment in mice with photoallergy. Sunscreens are recommended for protection against UV light–induced skin damage, but treatment of the skin with products containing antioxidant ingredients, such as tocopherols and ascorbate polyphenols, also be a useful strategy for the prevention of UV-mediated cutaneous damage. Broad-spectrum sunscreens are needed for protection against UVA. Therefore, it is suggested that nano-Pt demonstrating high antioxidant and antiinflammatory effects may have utility as a new class of sunscreens aimed at reducing ROS in the skin caused by UV exposure.

In conclusion, this study demonstrates that nano-Pt are effective in reducing UV-induced ROS and apoptosis and that topically applied nano-Pt effectively protects against UV-induced skin inflammation and photoallergy. Thus, we speculate that nano-Pt gel could be a useful sunscreen product for human skin therapy in the near future by providing effective protection against photo damage.

Acknowledgement

This research was supported by a Grant-in-Aid for research (No. 20591337) from the Ministry of Education, Science, and Culture of Japan.

Conflict of interest

The authors state no conflict of interest.

References

1 Peus D, Vasa R A, Meves A *et al.* H2O2 is an important mediator of UVB-induced EGF-receptor phosphorylation in cultured keratinocytes. J Invest Dermatol 1998: **110**: 966–971.
2 Ichihashi M, Ueda M, Budiyanto A *et al.* UV-induced skin damage. Toxicology 2003: **189**: 21–39.
3 Halliday G M. Inflammation, gene mutation and photoimmunosuppression in response to UVR-induced oxidative damage contributes to photocarcinogenesis. Mutat Res 2005: **571**: 107–120.
4 Bokov A, Chaudhuri A, Richardson A. The role of oxidative damage and stress in aging. Mech Ageing Dev 2004: **125**: 811–826.
5 Halliwell B. Antioxidant defence mechanisms: from the beginning to the end (of the beginning). Free Radic Res 1999: **31**: 261–272.
6 Saija A, Tomaino A, Trombetta D, Giacchi M, De Pasquale A, Bonina F. Influence of different penetration enhancers on in vitro skin permeation and in vivo photoprotective effect of flavonoids. Int J Pharm 1998: **175**: 85–94.
7 Casagrande R, Georgetti S R, Verri W A Jr, Dorta D J, dos Santos A C, Fonseca M J. Protective effect of topical formulations containing quercetin against UVB-induced oxidative stress. J Photochem Photobiol B 2006: **84**: 21–27.
8 Kajita M, Hikosaka K, Iitsuka M, Kanayama A, Toshima N, Miyamoto Y. Platinum nanoparticle is a useful scavenger of superoxide anion and hydrogen peroxide. Free Radic Res 2007: **41**: 615–626.
9 Boukamp P, Petrussevska R T, Breitkreutz D, Hornung J, Markham A, Fusenig N E. Normal keratinization in a spontaneously immortalized aneuploid human keratinocyte cell line. J Cell Biol 1998: **106**: 761–771.
10 Li F J, Kondo T, Zhao Q L *et al.* Enhancement of hyperthermia-induced apoptosis by a free radical initiator 2,2′-azobis (2-amidinopropane) dihydrochloride, in human histiocytic lymphoma U937 cells. Free Radic Res 2001: **35**: 281–299.
11 Sellins K S, Cohen J J. Gene induction by gamma-irradiation leads to DNA fragmentation in lymphocytes. J Immunol 1987: **139**: 3199–3206.
12 Hirano H, Tabuchi Y, Kondo T *et al.* Analysis of gene expression in apoptosis of human lymphoma U937 cells induced by heat shock and the effects of α-phenyl *N*-tert-butylnitrone (PBN) and its derivates. Apoptosis 2005: **10**: 331–340.
13 Zhao Q L, Fujiwara Y, Kondo T. Mechanism of cell death induction by nitroxide and hyperthermia. Free Radic Biol Med 2006: **40**: 1131–1143.
14 Lee E H, Faulhaber D, Hanson K M *et al.* Dietary lutein reduces ultraviolet radiation-induced inflammation and immunosuppression. J Invest Dermatol 2004: **122**: 510–517.
15 Tokura Y, Seo N, Yagi H, Furukawa F, Takigawa M. Cross-reactivity in murine fluoroquinolone photoallergy: exclusive usage of TCR Vbeta13 by immune T cells that recognize fluoroquinolone-photomodified cells. J Immunol 1998: **160**: 3719–3728.
16 Cui Z G, Kondo T, Ogawa R *et al.* Enhancement of radiation-induced apoptosis by 6-formylpterin. Free Radic Res 2004: **38**: 363–373.
17 Matsumura Y, Ananthaswamy H N. Toxic effects of ultraviolet radiation on the skin. Toxicol Appl Pharmacol 2004: **195**: 298–308.
18 Morganti P, Bruno C, Guarneri F, Cardillo A, Del Ciotto P, Valenzano F. Role of topical and nutritional supplement to modify the oxidative stress. Int J Cosmet Sci 2002: **24**: 331–339.
19 Sadrieh N, Wokovich A M, Gopee N V *et al.* Lack of significant dermal penetration of titanium dioxide (TiO_2) from sunscreen formulations containing nano- and sub-micron-size TiO_2 particles. Toxicol Sci 2010: **15**: 156–166.
20 Onizawa S, Aoshiba K, Kajita M, Miyamoto Y, Nagai A. Platinum nanoparticle antioxidants inhibit pulmonary inflammation in mice exposed to cigarette smoke. Pulm Pharmacol Ther 2009: **22**: 340–349.
21 Kim J, Takahashi M, Shimizu T *et al.* Effects of a potent antioxidant, platinum nanoparticle, on the lifespan of Caenorhabditis elegans. Mech Ageing Dev 2008: **129**: 322–331.
22 Woelfle U, Laszczyk M N, Kraus M *et al.* Triterpenes promote keratinocyte differentiation in vitro, ex vivo and in vivo: a role for the transient receptor potential canonical (subtype) 6. J Invest Dermatol 2009: **130**: 113–123.
23 Heinrich A, Balszuweit F, Thiermann H, Kehe K. Rapid simultaneous determination of apoptosis, necrosis, and viability in sulfur mustard exposed HaCaT cell cultures. Toxicol Lett 2009: **191**: 260–267.
24 Ayala F, Grimaldi E, Perfetto B *et al.* A 5-Aminolaevulinic acid and photodynamic therapy reduce HSV-1 replication in HaCat cells through an apoptosis-independent mechanism. Photodermatol Photoimmunol Photomed 2008: **24**: 237–243.
25 He Y -Y, Huang J -L, Colin CF. Delayed and sustained activation of extracellular signal-regulated kinase in human keratinocytes by UVA. J Biol Chem 2004: **279**: 53867–53874.
26 Bachelor M A, Bowden G T. Ultraviolet A-induced Modulation of Bcl-XL by p38 MAPK in Human Keratinocytes J Biol Chem 2004: **279**: 42658–42668.
27 Fujita A, Maruyama M, Araya J *et al.* Hydrogen peroxide induces upregulation of Fas in human airway epithelial cells via the activation of PARP-p53 pathway. Am J Respir Cell Mol Biol 2002: **27**: 542–552.
28 Kiss B, Bíró T, Czifra G *et al.* Investigation of micronized titanium dioxide penetration in human skin xenografts and its effect on cellular functions of human skin-derived cells. Exp Dermatol 2008: **17**: 659–667.
29 Thiele J J, Podda M, Packer L. Tropospheric ozone: an emerging environmental stress to skin. Biol Chem 1997: **378**: 1299–1305.
30 Tokura Y. Quinolone photoallergy: photosensitivity dermatitis induced by systemic administration of photohaptenic drugs. J Dermatol Sci 1998: **18**: 1–10.

Supporting Information

Additional Supporting Information may be found in the online version of this article:

Figure S1. Effects of nano-Pt on reactive oxygen species production.

Figure S2. Nano-Pt suppression of UVB-mediated inflammation in mice.

Figure S3. Nano-Pt suppression of photoallergy.

Please note: Wiley-Blackwell are not responsible for the content or functionality of any supporting materials supplied by the authors. Any queries (other than missing material) should be directed to the corresponding author for the article.

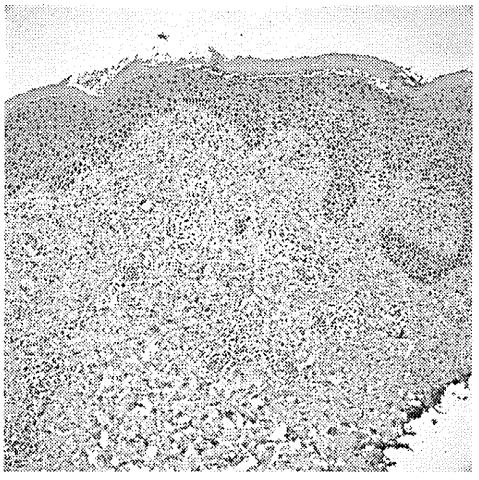

Fig 2. Immunohistochemistry of skin for angiopoietin-2. Note the abundant staining in the basal epidermis and dermal inflammatory cells. (Original magnification: ×100.)

National Institutes of Health, and a Veterans Administration Hospital Merit Award (to J.L.A.)

Conflicts of interest: None declared.

Reprint requests: Jack L. Arbiser, MD, PhD, Department of Dermatology, Emory University School of Medicine, WMB 5309, 1639 Pierce Dr, Atlanta, GA 30322.

E-mail: jarbise@emory.edu

REFERENCES

1. Bhandarkar SS, MacKelfresh J, Fried L, Arbiser JL. Targeted therapy of oral hairy leukoplakia with gentian violet. J Am Acad Dermatol 2008;58:711-2.
2. Lambeth JD, Kawahara T, Diebold B. Regulation of Nox and Duox enzymatic activity and expression. Free Radic Biol Med 2007;43:319-31.
3. Perry BN, Govindarajan B, Bhandarkar SS, Knaus UG, Valo M, Sturk C, et al. Pharmacologic blockade of angiopoietin-2 is efficacious against model hemangiomas in mice. J Invest Dermatol 2006;126:2316-22.
4. Brockow K, Grabenhorst P, Abeck D, Traupe B, Ring J, Hoppe U, et al. Effect of gentian violet, corticosteroid and tar preparations in *Staphylococcus aureus*—colonized atopic eczema. Dermatology 1999;199:231-6.
5. Howell MD, Novak N, Bieber T, Pastore S, Girolomoni G, Boguniewicz M, et al. Interleukin-10 downregulates anti-microbial peptide expression in atopic dermatitis. J Invest Dermatol 2005;125:738-45.

doi:10.1016/j.jaad.2009.05.027

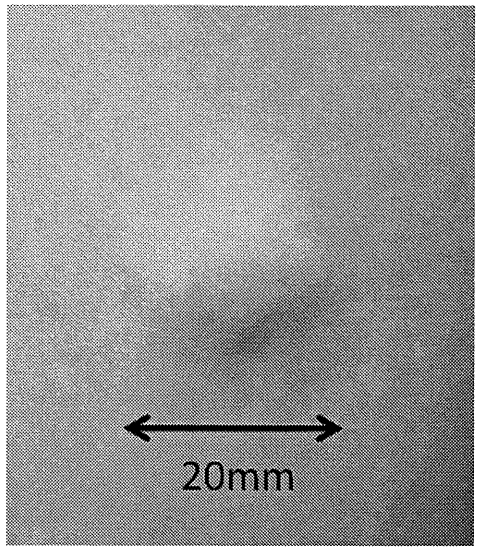

Fig 1. A slightly violaceous nodule on the middle aspect of the left thigh.

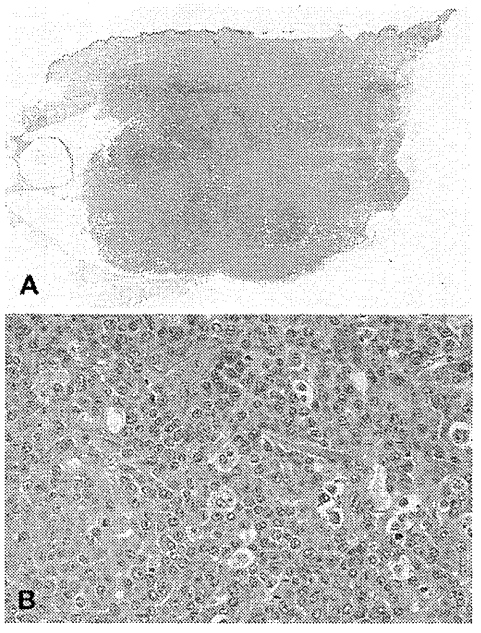

Fig 2. Skin biopsy findings. **A**, Dense, nodular, diffuse infiltrate of monotonous uniform cells involving the dermis and subcutaneous fat. **B**, A nodule of cells with round nuclei; prominent single or multiple nucleoli; abundant pale, slightly eosinophilic cytoplasm; and a number of atypical mitotic figures.

Aleukemic leukemia cutis with extensive bone involvement

To the Editor: Aleukemic leukemia cutis (ALC) is a rare condition that is characterized by the invasion of leukemic cells into the skin before such cells are observed in the peripheral blood.[1] We present a case of ALC with multiple bone metastases.

An 81-year-old man had a 2-month history of asymptomatic nodules on his trunk and legs. The physical examination revealed five subcutaneous nodules measuring up to 10 mm in size on his back and legs and a firm, slightly violaceous nodule

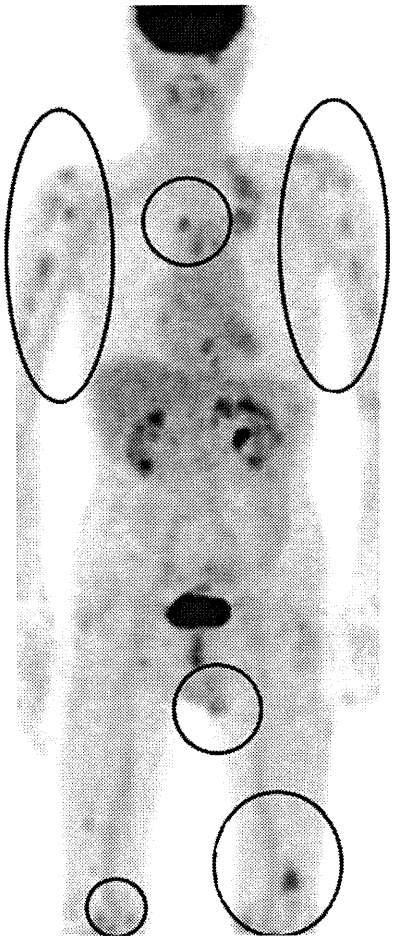

Fig 3. A positron emission tomography scan reveals extensive high-density areas in the bone and in the subcutaneous tissue of the trunk and the extremities, suggesting multiple metastases.

measuring 20 mm in diameter on the middle aspect of his left thigh (Fig 1). A complete blood cell count and chemical analysis showed no pathologic changes. Histopathologic examination of a skin biopsy specimen revealed a dense, nodular, diffuse infiltrate of monotonous uniform cells with round nuclei, prominent single or multiple nucleoli, and abundant pale, slightly eosinophilic cytoplasmic cells throughout the dermis and subcutaneous fat (Fig 2, *A*). A number of atypical mitotic figures were seen (Fig 2, *B*). The tumor cells were positive for leukocyte common antigen, CD68, and myeloperoxidase. A histologic diagnosis of myeloid leukemia cutis with possible monocytic lineage was made. However, bone marrow aspiration showed neither an increase in blasts nor abnormal cell infiltration, and repeated peripheral blood cell counts were normal, with no atypical cells. A diagnosis of ALC was established. Positron emission tomography (PET) revealed extensive high-density areas in the bone and subcutaneous tissue, suggesting multiple metastases (Fig 3). Seven weeks after his first visit, a peripheral blood cell examination disclosed 8% atypical monocytic cells, suggesting a diagnosis of acute myeloid leukemia. The patient refused other studies and died 1 week later.

ALC is a rare form of leukemia with a poor prognosis. The term "aleukemic" has been used to designate a form of leukemia in which there are no leukemic cells in the blood.[2] ALC precedes peripheral blood or bone marrow abnormalities at least 1 month before the systemic findings. Once leukemic cells appear in the peripheral blood or bone marrow, the mean survival time ranges from 3 to 30 months.[3,4] The clinical features of ALC include multiple papules, nodules, or infiltrated plaques with a red-brown or plum-colored surface. Histologic findings show the infiltration of leukemic cells in the dermal or subcutaneous tissues. The cytologic features of the tumor cells include large, vesicular nuclei and multiple prominent nucleoli.[3] Because of the rarity of the disease, there is no consensus on the treatment of choice for ALC; radiotherapy, chemotherapy, and total body electron therapy have achieved variable results.[1,3-8] A study by Chang et al[4] of a large group of ALC patients showed that the most common extramedullary site of involvement after the skin (31 of 31 patients) was the lymph nodes (8 of 31 patients) followed by the spleen (2 of 31 patients). Although no reports of a clinical presentation of ALC with multiple sites of bone infiltration were found in a thorough search of the English-language literature, extramedullary leukemia is known to occur in bone.[5] We emphasize that the routine assessment of a patient with ALC should include systemic investigations such as PET, taking into consideration the possibility of bone involvement.

Maria Maroto Iitani, MD, MSc,[a] Riichiro Abe, MD, PhD,[a] Teruki Yanagi, MD,[a] Asuka Hamasaka, MD, PhD,[a] Yasuki Tateishi, MD, PhD,[a] Yukiko Abe, MD, PhD,[a] Miki Ito, MD,[b] Takeshi Kondo, MD, PhD,[c] Kanako Kubota, MD, PhD,[d] and Hiroshi Shimizu, MD, PhD[a]

Departments of Dermatology, Hokkaido University Graduate School of Medicine[a] and the National Hospital Organization Hokkaido Cancer Center[b]; Departments of Gastroenterology and Hematology,[c] Hokkaido University Graduate School of Medicine; and the Department of Surgical Pathology,[d] Hokkaido University Hospital, Sapporo, Japan

Funding sources: None.

Conflicts of interest: None declared.

Reprint requests: Maria Maroto Iitani, MD, MSc, Department of Dermatology, Hokkaido University Graduate School of Medicine, North 15, West 7, Kita-ku, Sapporo 060-8638, Japan.

E-mail: miitani@med.hokudai.ac.jp

REFERENCES

1. Ohno S, Yokoo T, Ohta M, Yamamoto M, Danno K, Hamato N, et al. Aleukemic leukemia cutis. J Am Acad Dermatol 1990;22 (2 pt 2):374-7.
2. Yoder FW, Shuen RL. Aleukemic leukemia cutis. Arch Dermatol 1976;112:367-9.
3. Okun MM, Fitzgibbon J, Nahass GT, Forsman K. Aleukemic leukemia cutis, myeloid subtype. Eur J Dermatol 1995;5:290-3.
4. Chang H, Shih LY, Kuo TT. Primary aleukemic myeloid leukemia cutis treated successfully with combination chemotherapy: report of a case and review of the literature. Ann Hematol 2003;82:435-9.
5. Lee B, Fatterpekar GM, Kim W, Som PM. Granulocytic sarcoma of the temporal bone. AJNR Am J Neuroradiol 2002;23:1497-9.
6. Török L, Lueff S, Garay G, Tápai M. Monocytic aleukemic leukemia cutis. J Eur Acad Dermatol Venerol 1999;13:54-8.
7. Tomasini C, Quaglino P, Novelli M, Fierro MT. "Aleukemic" granulomatous leukemia cutis. Am J Dermatopathol 1998;20:417-21.
8. Imanaka K, Fujiwara K, Satoh K, Kuroda Y, Takahashi M, Sadatoh N, et al. A case of aleukemic monocytic leukemia cutis treated with total body electron therapy. Radiat Med 1988;6:229-31.

doi:10.1016/j.jaad.2009.05.040

Onychopapilloma presenting as longitudinal leukonychia

To the Editor: Onychopapilloma is an uncommon benign nail neoplasm characterized histologically by distal subungal hyperkeratosis and nail matrix metaplasia of the nail bed with marked papillomatosis. The majority of cases present clinically as localized longitudinal erythronychia. We report a case of onychopapilloma presenting as localized longitudinal leukonychia.

A 50-year-old woman was referred for the evaluation of dystrophy of the right third fingernail. The nail plate had split distally for several years. Her medical history was noncontributory. The physical examination revealed a 1-mm wide band of longitudinal leukonychia with a slight longitudinal ridge on the right third fingernail. No erythronychia was present. Distally, there was a V-shaped notch and split, with a keratotic 1-mm papule at the hyponychium (Fig 1). The other nails were normal. Lateral nail plate curl avulsion exposed a longitudinal ridge extending from the midmatrix onto the nail bed. A longitudinal biopsy from matrix to hyponychium was performed. On histologic examination, the nail bed exhibited slender, elongated, and hyperplastic rete ridges with underlying fibrosis and thickening of the fibrovascular dermal stroma. Upper nail bed keratinocytes were large and exhibited ample pink cytoplasm similar to the nail matrix keratogenous zone. Hyperkeratosis was seen at the hyponychium (Fig 2). A periodic acid–Schiff test did not reveal fungal elements. These findings were consistent with the diagnosis of onychopapilloma.

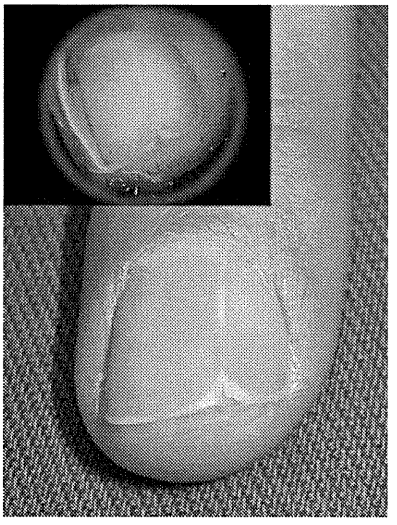

Fig 1. Fingernail with a 1-mm wide band of longitudinal leukonychia and distal V-shaped splitting, onycholysis, and a keratotic papule at the free edge of the nail. Dermatoscopy highlights these findings (*inset*).

Onychopapilloma was first reported in 1995 by Baran and Perrin,[1] who described four cases of "distal subungual keratosis with multinucleate cells." The term "onychopapilloma" was later coined in 2000 when the authors reported a second series of 14 cases with similar clinical and histopathologic features.[2] Key among these features were the upper cell layers in the nail bed epithelium exhibiting abundant eosinophilic cytoplasm resembling the nail matrix keratogenous zone, and was thought to indicate matrix metaplasia of the nail bed epithelium. Additional findings included acanthosis and papillomatosis of the distal nail bed epithelium. Multinucleated cells were found variably. In both series, all lesions presented as either longitudinal erythronychia or longitudinal bands of splinter hemorrhages, several of which were associated with distal onycholysis. Other occurrences of suspected onychopapilloma have been reported, including one case representing solitary nail bed lichen planus, and also in the spectrum of localized longitudinal erythronychia.[3] In addition to onychopapilloma, the differential diagnosis for localized longitudinal erythronychia includes Bowen disease,[2,3] and histologic investigation is often warranted.

severe chronic upper airway disease (SCUAD). J Allergy Clin Immunol 2009;124: 428-33.
4. Okano M, Fujiwara T, Haruna T, Kariya S, Makihara S, Higaki T, et al. PGE_2 suppresses staphylococcal enterotoxin-induced eosinophilia-associated cellular responses dominantly via an EP2-mediated pathway in nasal polyps. J Allergy Clin Immunol 2009;123:868-74.
5. Bachert C, Zhang N, van Zele T, Gevaert P, Patou J, van Cauwenberge P. *Staphylococcus aureus* enterotoxins as immune stimulants. In: Halilos DL, Baroody FM, editors. Chronic rhinosinusitis. Pathogenesis and medical management. New York: Informa Healthcare USA; 2007. p. 163-75.
6. Napolitani G, Acosta-Rodriguez EV, Lanzavecchia A, Sallusto F. Prostaglandin E_2 enhances Th17 responses via modulation of IL-17 and IFN-γ production by human CD4+ T cells. Eur J Immunol 2009;39:1-12.
7. Saito T, Kusunoki T, Yao T, Kawano K, Kojima Y, Miyahara K, et al. Role of interleukin-17A in the eosinophil accumulation and mucosal remodeling in chronic rhinosinusitis with nasal polyps associated with asthma. Int Arch Allergy Immunol 2009;151:8-16.
8. Su YC, Rolph MS, Hansbro NG, Mackay CR, Sewell WA. Granulocyte-macrophage colony-stimulating factor is required for bronchial eosinophilia in a murine model of allergic airway inflammation. J Immunol 2008;180:2600-7.
9. Doganci A, Eigenbrod T, Krug N, De Sanctis GT, Hausding M, Erpenbeck VJ, et al. The IL-6R alpha chain controls lung CD4+CD25+ Treg development and function during allergic airway inflammation in vivo. J Clin Invest 2005; 115:313-25.

Available online July 12, 2010.
doi:10.1016/j.jaci.2010.05.014

Topical application of dehydroxymethylepoxyquinomicin improves allergic inflammation via NF-κB inhibition

To the Editor:

Atopic dermatitis (AD) is a chronic, relapsing inflammatory skin disease with significant morbidity and an adverse impact on patient well-being. AD has become increasingly prevalent in industrialized countries, where it now occurs in 10% to 20% of children and 1% to 3% adults.[1] Corticosteroids are generally prescribed to control the symptoms, yet repeated use can cause severe skin atrophy and susceptibility to infection.[2] Tacrolimus, a calcineurin inhibitor, has recently gained widespread use as an AD treatment that avoids the typical side effects associated with topical corticosteroids.[3] However, refractory AD can remain even in patients treated with both corticosteroid and tacrolimus.

Dehydroxymethylepoxyquinomicin (DHMEQ), a newly developed low-molecular-weight nuclear factor- κB (NF-κB) inhibitor, is a 5-dehydroxymethyl derivative of the antibiotic epoxyquinomicin C.[4] DHMEQ has been found to inhibit TNF-α–induced NF-κB activation by suppressing nuclear translocation but not IκB phosphorylation or degradation.[5] Recently the antitumor effects of DHMEQ on breast,[6] thyroid,[7] and prostate[8] cancers as well as its anti-inflammatory and immunosuppressive effects have been reported in mice models.[9,10] In this study, we used atopic dermatitis model mice to examine the antiallergic inflammation efficacy of DHMEQ.

We confirmed that DHMEQ effectively inhibited the NF-κB activity in macrophage-like cell line, RAW264.7 with LPS stimulation (Fig 1, *A*).

First we examined whether DHMEQ suppressed contact hypersensitivity response. Balb/c mice were sensitized with 2,4,6-trinitrochlorobenzene (TNCB) to the dorsal skin and challenged 5 days later on the dorsal surface of the right ear. Immediately after the challenge, DHMEQ (1 mg/mL in acetone) or tacrolimus ointment (1%) was applied to the same ear. The DHMEQ-treated ears showed significantly less ear swelling than the tacrolimus-treated ears (Fig 1, *B*). The suppressive effect of DHMEQ was dose-dependent (Fig 1, *C*). Furthermore, expression of inflammatory cytokine mRNA (IL-1β, IL-6, TNF-α) in lesional skin was suppressed by DHMEQ ointment as well as by tacrolimus ointment (Fig 1, *D*). These data show that DHMEQ suppresses inflammation via suppression of inflammatory cytokine expression regulated by NF-κB.

We next examined whether DHMEQ would inhibit hapten-induced Langerhans cell (LC) migration. Treatment with TNCB caused a significant decline in epidermal LC density 4 hours after application in the untreated mice (30.5%). In contrast, TNCB treatment failed to provoke a significant epidermal LC migration response in the DHMEQ-treated mice (13.1%; Fig 1, *E*). We further evaluated LC morphology in the epidermal sheet preparations derived from the untreated and DHMEQ-treated mice. As illustrated in Fig 1, *F (left)*, at 4 hours after exposure to TNCB, the LCs in the control mice appeared to be activated and to have extended dendritic processes, whereas no such morphologic changes were evident in the LCs examined in the DHMEQ-treated mice (Fig 1, *F, right*). These data support that the DHMEQ suppressed the contact hypersensitivity response at least in part by inhibition of LC migration.

To determine whether DHMEQ has any therapeutic effect in AD, we applied DHMEQ to AD-like lesions of NC/Nga mice and evaluated the progression of skin changes. NC/Nga mice were the spontaneous mouse models of AD. Another spontaneous mouse model, the DS-Nh mouse, has a mutation of transient receptor potential vanilloid 3,[11] whereas the genetic defect of NC/Nga is not known. We used conventional NC/Nga mice that presented severe skin lesions very similar to those of human AD.[12] Conventional NC/Nga mice with moderate to severe AD were topically applied with 1% DHEMQ in plastibase (5% polyethylene and 95% mineral oil), 0.1% tacrolimus ointment, or 0.12% betamethasone ointment daily for 2 weeks. The clinical severity of skin lesion was scored daily according to the 5 main clinical symptoms: scratch behavior, erythema/hemorrhaging, edema, excoriation/erosion, and scaling/dryness.[12] Topical DHMEQ application significantly improved the severity of skin lesions compared with the ointment base as well compared with topical treatment with the 0.1% tacrolimus or 0.12% betamethasone ointment (Fig 2, *A and B*). Improvement of clinical skin condition by DHMEQ was also confirmed by histologic observation, which showed amelioration of hyperkeratosis, acanthosis, dermal edema, and infiltration of the inflammatory cells compared with the ointment base treatment (Fig 2, *C*). At the affected skin sites, the numbers of eosinophils and mast cells were significantly lower in the DHMEQ-treated mice than those in the control mice (Fig 2, *C*).

Potential side effects of topical application of NF-κB inhibition might include susceptibility to infection via local immune suppression. However NF-κB inhibitor presumably avoids the typical side effects associated with topical corticosteroids as well as tacrolimus.

Several reagents targeting NF-κB have been reported. For example, NF-κB decoy oligodeoxynucleotides were reported to be effective in resolving atopic skin lesions in NC/Nga mice.[13] IMD-0354, a selective IKK inhibitor, also improved AD manifestation in model mice.[14] In contrast with these, DHMEQ inhibits NF-κB activation by suppressing nuclear translocation but not IκB phosphorylation or degradation.[5] Because DHMEQ has a unique mechanism to inhibit NF-κB activation, DHMEQ might be effective for AD that does not respond to tacrolimus or corticosteroid, and it might have additive effects with other reagents.

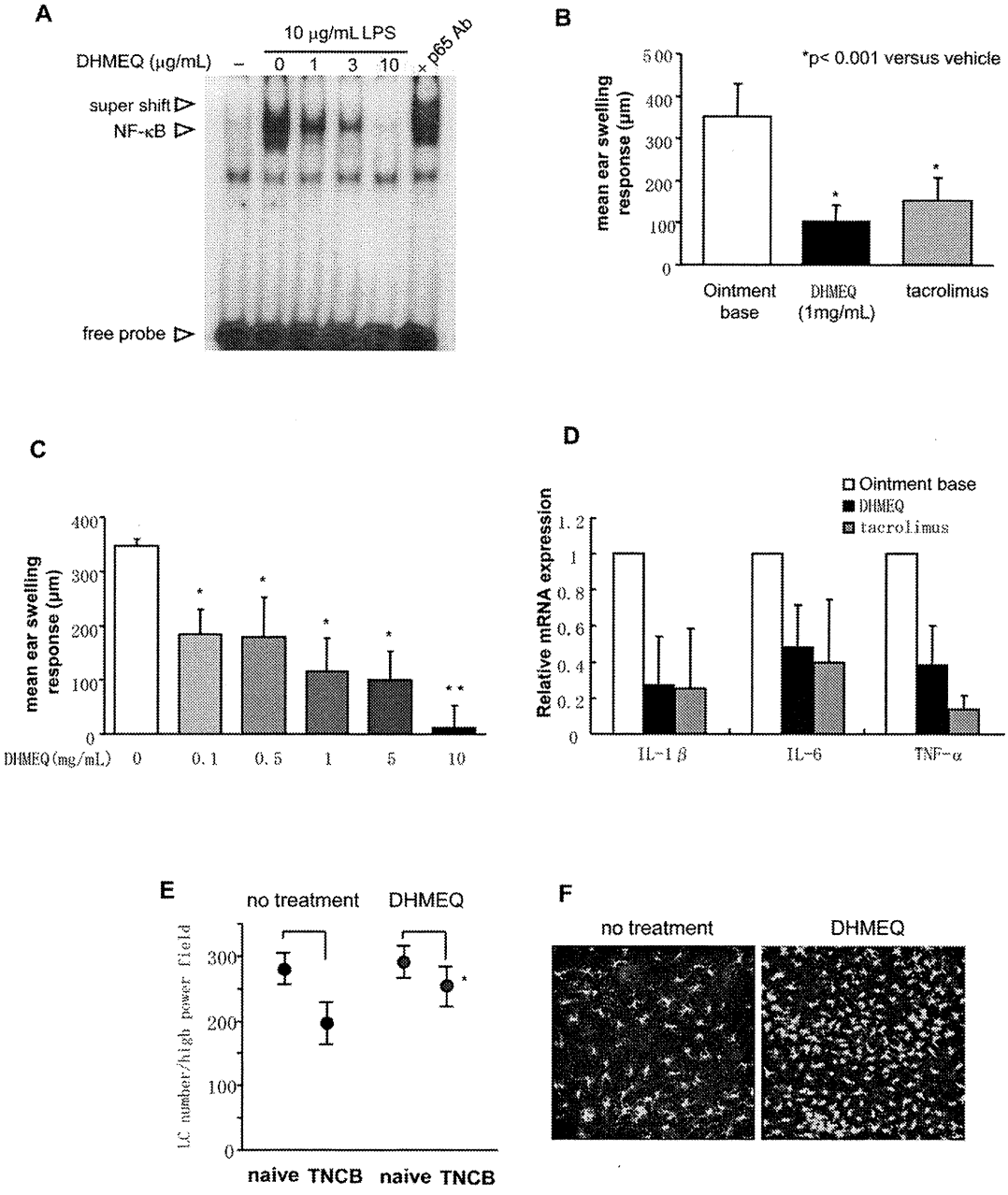

FIG 1. Effect of DHMEQ on contact hypersensitivity response. **A,** DHMEQ effectively inhibited the NF-κB activity in macrophagelike cell line RAW264.7 with LPS stimulation (10 μg/mL). **B,** DHMEQ, tacrolimus, or ointment base was applied topically. All ear-swelling values are shown as means ± SEs (n = 5). $*P < .01$; $**P < .005$. **C,** DHMEQ was applied in various concentrations. **D,** The density of mRNA expression of skin was analyzed by RT-PCR. **E,** The number of LCs was counted. $*P < .05$ (n = 4 for each group). **F,** LC morphology in epidermal sheet preparations derived from untreated *(left)* and DHMEQ-treated *(right)* mice.

In conclusion, we clearly demonstrated that DHMEQ inhibits the contact hypersensitivity response via suppression of inflammatory cytokines and decrease in LC migration. Furthermore, DHMEQ was found to improve AD manifestation of model mice with an efficacy equivalent to that of tacrolimus or betamethasone. DHMEQ may offer a novel therapeutic approach for the treatment of AD.

Asuka Hamasaka, MD, PhD[a]*
Naoya Yoshioka, MS[a]*
Riichiro Abe, MD, PhD[a]
Satoshi Kishino, PhD[d]
Kazuo Umezawa, MD, PhD[e]
Michitaka Ozaki, MD, PhD[b]
Satoru Todo, MD, PhD[c]
Hiroshi Shimizu, MD, PhD[a]

From [a]the Department of Dermatology, [b]the Department of Molecular Surgery, and [c]the First Department of Surgery, Hokkaido University Graduate School of Medicine, Sapporo; [d]the Department of Medication Use Analysis and Clinical Research, Meiji Pharmaceutical University, Tokyo; and [e]the Department of Applied Chemistry, Keio

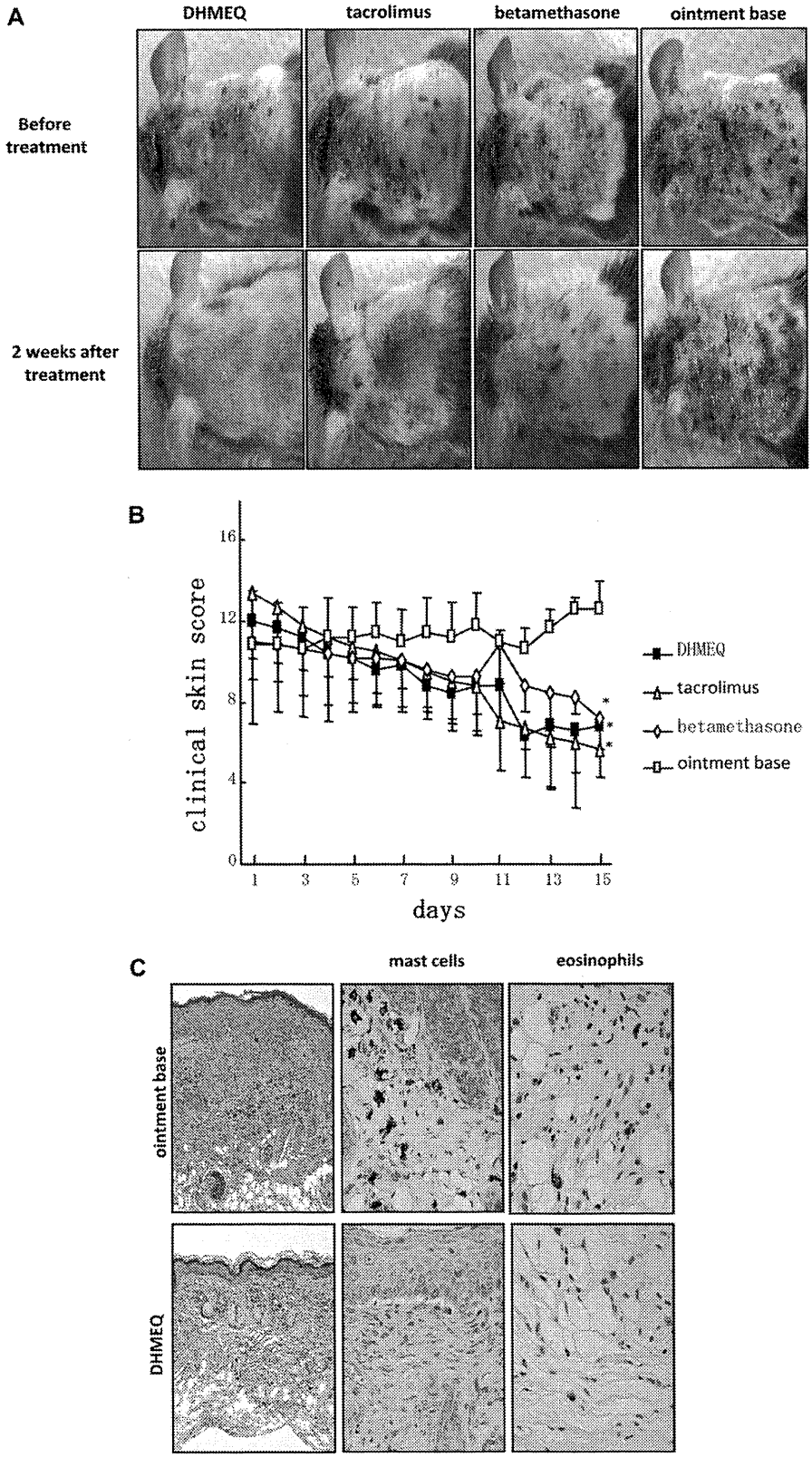

FIG 2. Improvement of atopic dermatitis model mice by DHMEQ. NC/Nga mice were applied topically with DHMEQ, tacrolimus, or ointment base. **A,** Clinical features of each mouse. **B,** The clinical skin score of each group is given as mean ± SE. *$P < .005$. **C,** Specimens were collected from the dorsal skin and were stained with hematoxylin and eosin, direct fast scarlet for eosinophils, or toluidine blue for mast cells.

University, Yokohama, Japan. E-mail: aberi@med.hokudai.ac.jp, shimizu@med.hokudai.ac.jp.

Disclosure of potential conflict of interest: This study was supported by the Program for Promotion of Fundamental Studies in Health Sciences of the National Institute of Biomedical Innovation (NIBIO).

*These authors contributed equally to this work.

REFERENCES

1. Morar N, Willis-Owen SA, Moffatt MF, Cookson WO. The genetics of atopic dermatitis. J Allergy Clin Immunol 2006;118:24-34, quiz 5-6.
2. Abramovits W, Perlmutter A. Steroids versus other immune modulators in the management of allergic dermatoses. Curr Opin Allergy Clin Immunol 2006;6:345-54.
3. El-Batawy MM, Bosseila MA, Mashaly HM, Hafez VS. Topical calcineurin inhibitors in atopic dermatitis: a systematic review and meta-analysis. J Dermatol Sci 2009;54:76-87.
4. Matsumoto N, Ariga A, To-e S, Nakamura H, Agata N, Hirano S, et al. Synthesis of NF-kappaB activation inhibitors derived from epoxyquinomicin C. Bioorg Med Chem Lett 2000;10:865-9.
5. Ariga A, Namekawa J, Matsumoto N, Inoue J, Umezawa K. Inhibition of tumor necrosis factor-alpha -induced nuclear translocation and activation of NF-kappa B by dehydroxymethylepoxyquinomicin. J Biol Chem 2002;277:24625-30.
6. Matsumoto G, Namekawa J, Muta M, Nakamura T, Bando H, Tohyama K, et al. Targeting of nuclear factor kappaB Pathways by dehydroxymethylepoxyquinomicin, a novel inhibitor of breast carcinomas: antitumor and antiangiogenic potential in vivo. Clin Cancer Res 2005;11:1287-93.
7. Starenki DV, Namba H, Saenko VA, Ohtsuru A, Maeda S, Umezawa K, et al. Induction of thyroid cancer cell apoptosis by a novel nuclear factor kappaB inhibitor, dehydroxymethylepoxyquinomicin. Clin Cancer Res 2004;10:6821-9.
8. Kikuchi E, Horiguchi Y, Nakashima J, Kuroda K, Oya M, Ohigashi T, et al. Suppression of hormone-refractory prostate cancer by a novel nuclear factor kappaB inhibitor in nude mice. Cancer Res 2003;63:107-10.
9. Wakamatsu K, Nanki T, Miyasaka N, Umezawa K, Kubota T. Effect of a small molecule inhibitor of nuclear factor-kappaB nuclear translocation in a murine model of arthritis and cultured human synovial cells. Arthritis Res Ther 2005;7:R1348-59.
10. Ueki S, Yamashita K, Aoyagi T, Haga S, Suzuki T, Itoh T, et al. Control of allograft rejection by applying a novel nuclear factor-kappaB inhibitor, dehydroxymethylepoxyquinomicin. Transplantation 2006;82:1720-7.
11. Asakawa M, Yoshioka T, Matsutani T, Hikita I, Suzuki M, Oshima I, et al. Association of a mutation in TRPV3 with defective hair growth in rodents. J Invest Dermatol 2006;126:2664-72.
12. Matsuda H, Watanabe N, Geba GP, Sperl J, Tsudzuki M, Hiroi J, et al. Development of atopic dermatitis-like skin lesion with IgE hyperproduction in NC/Nga mice. Int Immunol 1997;9:461-6.
13. Nakamura H, Aoki M, Tamai K, Oishi M, Ogihara T, Kaneda Y, et al. Prevention and regression of atopic dermatitis by ointment containing NF-kB decoy oligodeoxynucleotides in NC/Nga atopic mouse model. Gene Ther 2002;9:1221-9.
14. Tanaka A, Muto S, Jung K, Itai A, Matsuda H. Topical application with a new NF-kappaB inhibitor improves atopic dermatitis in NC/NgaTnd mice. J Invest Dermatol 2007;127:855-63.

Available online July 12, 2010.
doi:10.1016/j.jaci.2010.05.020

A novel non–IgE-mediated pathway of mite-induced inflammation

To the Editor:

In a recent article published in the *Journal of Immunology*, Barrett et al[1] demonstrated that mite and *Aspergillus fumigatus* extracts stimulate the production of cysteinyl leukotrienes from bone marrow–derived dendritic and pulmonary $CD11c^+$ cells through a glycan C–type lectin receptor (Dectin-2) interaction involving FcRγ and Syk signaling that activates arachidonic acid metabolism.

Previously, a number of clinical and experimental observations had called our attention to the existence of important connections between IgE-mediated diseases and leukotriene-mediated inflammation. We had observed that a large proportion of patients with hypersensitivity to nonsteroidal anti-inflammatory drugs (NSAIDs), a condition that is accompanied by increased production of leukotrienes, were atopic and had IgE-mediated sensitivity to mite allergens.[2] This observation has been recently confirmed in another study in which we found significantly increased total and mite-specific IgE levels in patients with NSAID hypersensitivity compared with those seen in healthy control subjects.[3] In tropical countries in which high relative humidity and temperature are optimal for mite proliferation, mite allergens are the main source of sensitization and allergic respiratory disease.

A second clinical observation, also reported by Spanish investigators and others, was that most patients with anaphylaxis after the ingestion of mite-contaminated foods frequently exhibit hypersensitivity to NSAIDs.[4] We designated the association of allergic rhinitis, aspirin/NSAID hypersensitivity, and severe reactions to mite-contaminated foodstuffs as a "new aspirin triad." To understand this association, we performed a study in collaboration with Canadian investigators in which it was demonstrated that mite allergenic extracts inhibited COX-1 *in vitro*. We postulated that mite-induced human allergic diseases could be accompanied, at least in a subset of the patient population, by a dysregulation of leukotriene biosynthesis, metabolism, or both similar to the disturbances described in patients with NSAID hypersensitivity.

In concordance with that hypothesis, various genetic polymorphisms that involve leukotriene C_4 (LTC_4) synthase and cysteinyl leukotriene receptors have been observed in patients with hypersensitivity to NSAIDs; in that context it is important to mention that so-called atopic genes are located in the 5q22-q35 region of human chromosome 5, close to the *LTC4S* gene.

Diverse lines of evidence also support a dysregulation of leukotriene pathways in subjects with mite allergy. Acevedo et al[5] described an association of the A-444C allele of the *LTC4S* gene and IgE response to mite allergens, and we have observed that NSAID-sensitive patients show stronger skin test responses and increased specific IgE antibodies to *Blomia tropicalis* than atopic non–NSAID-sensitive subjects.[3]

Cysteinyl leukotrienes modulate the allergic response, as evidenced in various studies in which it has been shown that leukotrienes enhance IgE and IgG production by human B cells, whereas *LTC4S* knockout mice have a markedly reduced antigen-induced T_H2 pulmonary inflammation. Additionally, it has been demonstrated that IL-4 and IL-13 modulate the number of cysteinyl leukotriene type 1 and 2 receptors on T, B, and antigen-presenting cells.

Furthermore, various groups of investigators have observed that aspirin enhances food-dependent exercise-induced anaphylaxis[6] and facilitates anaphylaxis induced by food allergens.[7-10] These effects could be due to an increased gut permeability, resulting in enhanced opportunity for sensitization at the immunocompetent cell–rich gastrointestinal submucosa.

Bachert et al[11] have proposed a role for staphylococcal enterotoxins, which, through the Vβ receptor on T lymphocytes, allow polyclonal IgE production, including IgE to house dust mite, in nasal polyps, the lungs, and possibly the skin. It would be interesting to investigate in the future whether aspirin-hypersensitive patients with urticaria and angioedema and those with oral anaphylaxis to mites have superantigen-induced immune stimulation

HUMAN MUTATION Mutation in Brief 31: E1687-E1698 (2010) Online

MUTATION IN BRIEF

HUMAN MUTATION

OFFICIAL JOURNAL HGVS HUMAN GENOME VARIATION SOCIETY www.hgvs.org

Plectin Deficiency Leads to Both Muscular Dystrophy and Pyloric Atresia in Epidermolysis Bullosa Simplex

Ken Natsuga[1]*, Wataru Nishie[1], Satoru Shinkuma[1], Ken Arita[1], Hideki Nakamura[1], Makiko Ohyama[2], Hitoshi Osaka[3], Takeshi Kambara[4], Yoshiaki Hirako[5], and Hiroshi Shimizu[1]

[1]Department of Dermatology, Hokkaido University Graduate School of Medicine, Sapporo, Japan; [2]Department of Pediatrics, Kanagawa Children's Medical Center, Yokohama, Japan; [3]Department of Neurology, Kanagawa Children's Medical Center, Yokohama, Japan; [4]Department of Dermatology, Yokohama City University School of Medicine, Yokohama, Japan; [5]Division of Biological Science, Graduate School of Science, Nagoya University, Nagoya, Japan

*Correspondence to Ken Natsuga, MD, PhD, Department of Dermatology, Hokkaido University Graduate School of Medicine, North 15 West 7, Sapporo 060-8638, Japan, Phone: +81-11-706-7387, Fax: +81-11-706-7820, E-mail: natsuga@med.hokudai.ac.jp

Communicated by Mireille Claustres

ABSTRACT: Plectin is a cytoskeletal linker protein which has a long central rod and N- and C-terminal globular domains. Mutations in the gene encoding plectin (*PLEC*) cause two distinct autosomal recessive subtypes of epidermolysis bullosa: EB simplex (EBS) with muscular dystrophy (EBS-MD), and EBS with pyloric atresia (EBS-PA). Previous studies have demonstrated that loss of full-length plectin with residual expression of the rodless isoform leads to EBS-MD, whereas complete loss or marked attenuation of expression of full-length and rodless plectin underlies the more severe EBS-PA phenotype. However, muscular dystrophy has never been identified in EBS-PA, not even in the severe form of the disease. Here, we report the first case of EBS associated with both pyloric atresia and muscular dystrophy. Both of the premature termination codon-causing mutations of the proband are located within exon 32, the last exon of *PLEC*. Immunofluorescence and immunoblot analysis of skin samples and cultured fibroblasts from the proband revealed truncated plectin protein expression in low amounts. This study demonstrates that plectin deficiency can indeed lead to both muscular dystrophy and pyloric atresia in an individual EBS patient.

KEY WORDS: basement membrane zone; skeletal muscle; mRNA decay; truncation

INTRODUCTION

Plectin is a 500-kDa protein of the plakin family, which interlinks different element of the cytoskeleton (Rezniczek, et al., 2010). Plectin is prominently expressed in muscle and in stratified and simple epithelia, including in the skin and gastrointestinal tract (Rezniczek, et al., 2010). In skin, plectin localizes to the inner plaque of the hemidesmosomes, at the site of interaction with intermediate filaments (Smith, et al., 1996). Plectin has a unique dumbbell-like structure with a central rod domain and N- and C-terminal globular domains (Wiche, et

Received 26 April 2010; accepted revised manuscript 7 July 2010.

DOI: 10.1002/humu.21330

al., 1991). Various types of plectin transcripts, including rodless ones, that do not encode for a central rod domain have been reported (Elliott, et al., 1997).

Epidermolysis bullosa (EB) comprises a group of heterogeneous congenital disorders characterized by dermal-epidermal junction separation. EB is subdivided into the three major groups of EB simplex (EBS), junctional EB and dystrophic EB, and the one minor group of Kindler syndrome, based on the level of blister formation (Fine, et al., 2008). So far, mutations in 14 different genes have been identified as underlying the EB subtypes (Fine, et al., 2008; Groves, et al., 2010). Among them, mutations in the gene encoding plectin, *PLEC* (MIM# 601282), have been known to be causal for two subtypes of autosomal recessive EBS (EBS with muscular dystrophy (EBS-MD) and EBS with pyloric atresia (EBS-PA)) and for one subtype of autosomal dominant EBS (EBS-Ogna) (Fine, et al., 2008).

Characteristic manifestations of EBS-MD are generalized skin blistering and late onset muscle weakness. Previous studies revealed defective expression of plectin in EBS-MD skin samples (Gache, et al., 1996; Shimizu, et al., 1999a; Shimizu, et al., 1999b) and mutations in *PLEC* in EBS-MD patients (McLean, et al., 1996; Pulkkinen, et al., 1996; Smith, et al., 1996; Takizawa, et al., 1999). The *PLEC* mutations detected in EBS-MD patients are mainly within exon 31, which encodes the large-rod domain of plectin (Natsuga, et al., 2010; Pfendner, et al., 2005; Sawamura, et al., 2007).

In contrast to patients with EBS-MD, those with EBS-PA typically develop a more severe phenotype that includes more generalized blistering and pyloric atresia (PA) (Nakamura, et al., 2005). The prognosis of EBS-PA is very poor, and affected patients usually die within months after birth (Nakamura, et al., 2005; Pfendner, et al., 2005; Pfendner and Uitto, 2005). *PLEC* mutations of EBS-PA were mostly located outside of exon 31 (Natsuga, et al., 2010).

Although both EBS-MD and EBS-PA are autosomal recessive EBS caused by *PLEC* mutations, the pathomechanisms distinguishing two subtypes were unclear. Recently, our group and others demonstrated that EBS-MD patients typically express a rodless plectin isoform, although the full-length plectin is absent (Koster, et al., 2004; Natsuga, et al., 2010). In contrast, both full-length and rodless plectin isoforms are deficient in EBS-PA patients, leading to the more severe disease phenotype (Natsuga, et al., 2010). In light of these findings, it has been postulated that EBS-PA patients could develop muscular dystrophy (MD) if they survived longer (Natsuga, et al., 2010). However, to our knowledge, there have been no EBS patients who suffered from both MD and PA.

Here, we report the first patient with EBS who developed both PA and MD. Both of the mutations identified in the patient were within the last exon (exon 32) of *PLEC*. Immunofluorescence and immunoblot analysis confirmed diminished and truncated plectin expression, using several antibodies against different domains of plectin. This study gives further insight toward improving our understanding of the genotype-phenotype correlation in EBS patients with *PLEC* mutations.

MATERIALS AND METHODS

Electron Microscopy

Skin biopsy samples were fixed in 2% glutaraldehyde solution, post-fixed in 1% OsO_4, dehydrated, and embedded in Epon 812. The samples were sectioned at 1 μm thickness for light microscopy and thin-sectioned for electron microscopy (70 nm thick). The thin sections were stained with uranyl acetate and lead citrate, and examined by transmission electron microscopy.

Mutation Detection

Genomic DNA (gDNA) was isolated from peripheral blood leukocytes of the proband and her parents. The mutation detection was performed after polymerase chain reaction (PCR) amplification of all *PLEC* exons and intron-exon borders, followed by direct automated sequencing using an ABI PRISM 3100 genetic analyzer (Applied Biosystems, Foster City, CA). The oligonucleotide primers and PCR conditions used in this study were derived from a previous report (Nakamura, et al., 2005). The gDNA nucleotides, the complementary DNA (cDNA)

nucleotides and the amino acids of the protein, were numbered based on the GenBank sequence information (accession no. NM_000445.3). PCR amplification of two parts of exon 32 was performed using the following primers. Primers 5'-GTGGAGACCACGCAGGTGTAC-3' and 5'-GGAGCCCGTGCCATAGAGG-3' for a single part of exon 32 synthesized a 420-bp fragment including c.10735 to c.11154. Primers 5'-AGCGGCTGACTGTGGATGAGG-3' and 5'-TGCGTGTCCTTGTTGAGGT-3' for another single part of exon 32 synthesized a 283-bp fragment including c.11230 to c.11512. Both of the mutations in the proband were confirmed by restriction digestion of PCR products. c.10984C>T and c.11453_11462del caused the generation of new restriction enzyme sites for *BsrI* and *BbvCI*, respectively.

The mutation nomenclature follows the journal's guidelines (www.hgvs.org/mutnomen) according to the reference sequence NM_000445.3, with +1 as the A of the ATG initiation codon.

Haplotype analysis

Genotype analysis of this family to establish the *de novo* nature of c.11453_11463del in the proband was performed using three chromosome 8 markers (D8S272, D8S264, D8S270) and six non-chromosome 8 markers (D1S468, D1S252, D1S2842, D3S1297, D3S1566 and D3S1311). All microsatellite markers (ABI Prism Linkage Mapping Set Version 2.5; Applied Biosystems, Warrington, UK) were amplified with fluorescently labeled oligonucleotides and used under conditions recommended by the manufacturer. Electrophoretic analysis was performed on an ABI Prism 310 Genetic Analyzer with Performance Optimized Polymer 4 (POP4) using GeneScan software (Applied Biosystems). The allele sizes were analyzed using Genotyper software (Applied Biosystems).

Immunofluorescence Studies

Immunofluorescence analysis was performed using skin specimens from the proband as previously described (Natsuga, et al., 2010). Briefly, fresh-frozen skin specimens were embedded in optimal cutting temperature (OCT) compound and quickly frozen in isopentane cooled over liquid nitrogen. 5-μm cryostat sections were incubated with primary antibodies. After washing in phosphate-buffered saline, the sections were incubated with secondary antibodies conjugated with fluorescein-isothiocyanate.

Antibodies

The following antibodies against basement membrane zone (BMZ) components were used: monoclonal antibody (mAb) PN643 against the N-terminal actin-binding domain of plectin; mAb HD1-121 against the rod domain of plectin; C20 and mAb PC-815 against the C-terminal globular domain of plectin (Fig. 1A); mAbs GoH3 and 3E1 (Chemicon International, CA) against α6 and ß4 integrins, respectively; mAb GB3 (Sera-lab, Cambridge, UK) against laminin 332; mAb LH7.2 (Sigma, St. Louis, MO) against type VII collagen; mAb PHM-12^{+}CIV22 against type IV collagen (NeoMarkers, Fremont, CA); and S1193 and mAb HDD20 against BP230 and type XVII collagen, respectively. mAbs PN643, HD1-121 and PC815 were generously donated by Prof. K. Owaribe of Nagoya University, and antibody S1193 by Prof. J. R. Stanley of the University of Pennsylvania. C20, a goat polyclonal antibody against the C-terminus of plectin, was purchased from Santa Cruz. Anti-beta-actin mAb (AC15, Sigma, St. Louis, MO) was used to confirm equal protein loading.

Cell Culture and Immunoblot Analysis

Cell culture and immunoblot analysis was performed as previously described (Natsuga, et al., 2010). Cultured fibroblasts were obtained from skin biopsies of a normal human volunteer and the proband. Cultured fibroblasts were maintained in Dulbecco's modified Eagle's medium supplemented with 10% (v/v) fetal bovine serum. For sample preparation, cultured cells were lysed in Nonidet-40 (NP-40) containing buffer (1% NP-40, 25mM Tris-HCl (pH 7.6), 4mM EDTA, 100mM NaCl, 1mM phenylmethylsulfonyl fluoride (PMSF), and proteinase inhibitor

cocktail (Sigma, St. Louis, MO)); cell debris was removed by centrifugation; and the supernatant was collected. Supernatants were boiled in Laemmli's sample buffer (Laemmli, 1970), applied to a 4–12% gradient Bis-Tris gel (Invitrogen, Carlsbad, CA), and transferred to a PVDF membrane. The membrane was incubated with PN643, HD1-121, C20 and AC15 followed by incubation with horseradish peroxidase (HRP) conjugated anti-mouse IgG (for PN643, HD1-121 and AC15) and HRP-conjugated anti-gout IgG (for C20). The blots were detected using ECL Plus Detection Kit (GE Healthcare, Fairfield, CT).

Semi-quantitative RT-PCR Analysis

Semi-quantitative reverse transcription PCR (RT-PCR) analysis was performed as previously described (Natsuga, et al., 2010). Total RNA was isolated from cultured fibroblasts (from normal human volunteers and the proband, using RNeasy kit (Qiagen, Valencia, CA)), and first-strand cDNA was made using Superscript III reverse transcriptase (Invitrogen, Carlsbad, CA). First-strand cDNA was then amplified by PCR with primers specific for the exon boundaries flanking the rod domain of plectin as described previously (Koster, et al., 2004; Natsuga, et al., 2010). The following primers were used (Fig. 1B): 30F, 5'-CATCAGCGAGACTCTGCGGC-3'; 31R, 5'-TGCGCCTGTCGCTTTTGTGC-3'; 31F, 5'-AGCTGGAGATGAGCGCTGA-3'; 32R, 5'-TGCTGCAGCTCCTCCTGC-3'. To ensure equal loading, a housekeeping gene (GAPDH) was simultaneously amplified. The PCR products were assessed on a 2% agarose gel. The images were obtained with LAS-4000 mini (Fujifilm, Tokyo, Japan).

The medical ethics committee of Hokkaido University Graduate School of Medicine approved all of the described studies. The study was conducted according to The Declaration of Helsinki Principles. Participants gave their written informed consent.

RESULTS

Case Description

The proband was a first child of non-consanguineous Japanese parents. There was no family history of bullous diseases. He was born by cesarean section after a 39-week gestation because of non-reassuring fetal status. Clinically the proband showed extensive blistering and aplasia cutis on the extremities (Fig. 2A, B). Routine abdominal X-ray revealed a single bubble sign, suggesting the presence of PA (Fig. 2C). Generalized muscle hypotonia, dysphagia and difficulty in breathing were also observed from birth. Laboratory examination at birth revealed markedly elevated levels of creatine kinase (CK) (11,852U/L, normal value; 60-400U/L). The skeletal muscle isoform of CK (CK-MM) was 84% of total CK (CK, 2058U/L at age 12 days). Elevated levels of muscle enzymes including CK and aldolase (normal value; 1.7-5.7U/L) persisted over the course of his life (CK, 1924U/L; aldolase, 40.0U/L at age 25 days). Based on the clinical features and laboratory data, the presence of MD was confirmed. Muscle biopsy and reconstructive surgery for PA was not performed because the parents did not consent. The proband died 3 months after birth. Permission for autopsy was refused.

Skin Separation in Basal Keratinocytes

Electron microscopy of the skin samples from the proband showed that the skin separation localized to the base of the basal keratinocytes (Fig. 2D). Hemidesmosomes were hypoplastic and found at the base of the intraepidermal split (Fig. 2D). Keratin clumps were not observed.

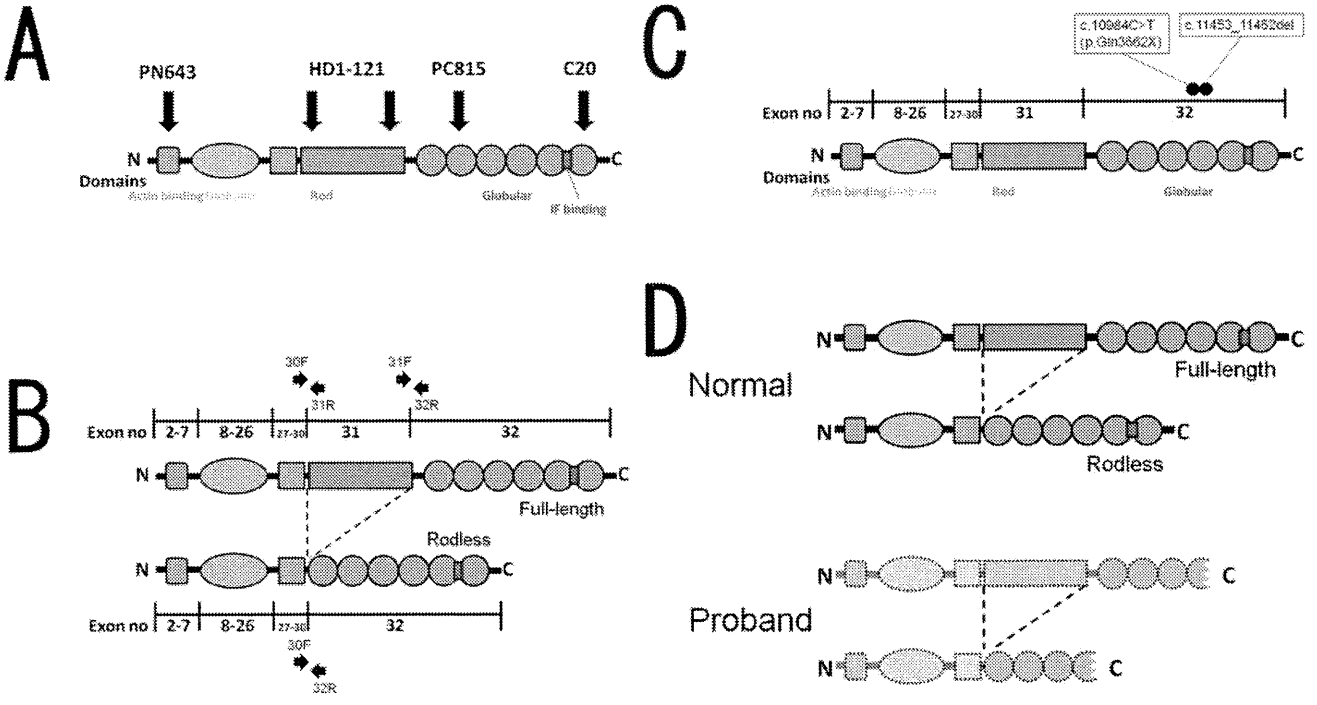

Figure 1. Plectin structure, antibodies against plectin, specific primers to amplify the full-length and the rodless plectin transcripts and *PLEC* mutations of the proband. (A) Plectin protein is composed of an actin-binding domain, N- and C-terminal globular domains, an intermediate filament (IF)-binding domain and a central rod domain. The C-terminal globular domain has 6 plectin repeat domains. The IF-binding domain is located between C-terminal repeats 5 and 6. PN643 is a monoclonal antibody (mAb) against the N-terminal actin-binding domain of plectin. HD1-121 is a mAb against the rod domain of plectin. PC815 is a mAb and C20 is a polyclonal antibody against the C-terminal globular domain of plectin. (B) The specific primers used to detect the presence of transcripts for full-length (30F/31R and 31F/32R) and rodless plectin (30F/32R) on cDNA synthesized from mRNA of normal humans and the proband's fibroblasts. (C) c.10984C>T and c.11453_11462del are located in the *PLEC* encoding C-terminal plectin repeat 4. (D) Normal humans express both full-length and rodless plectin. In our case, the *PLEC* mutations produced diminished and truncated plectin protein without the IF-binding domain.

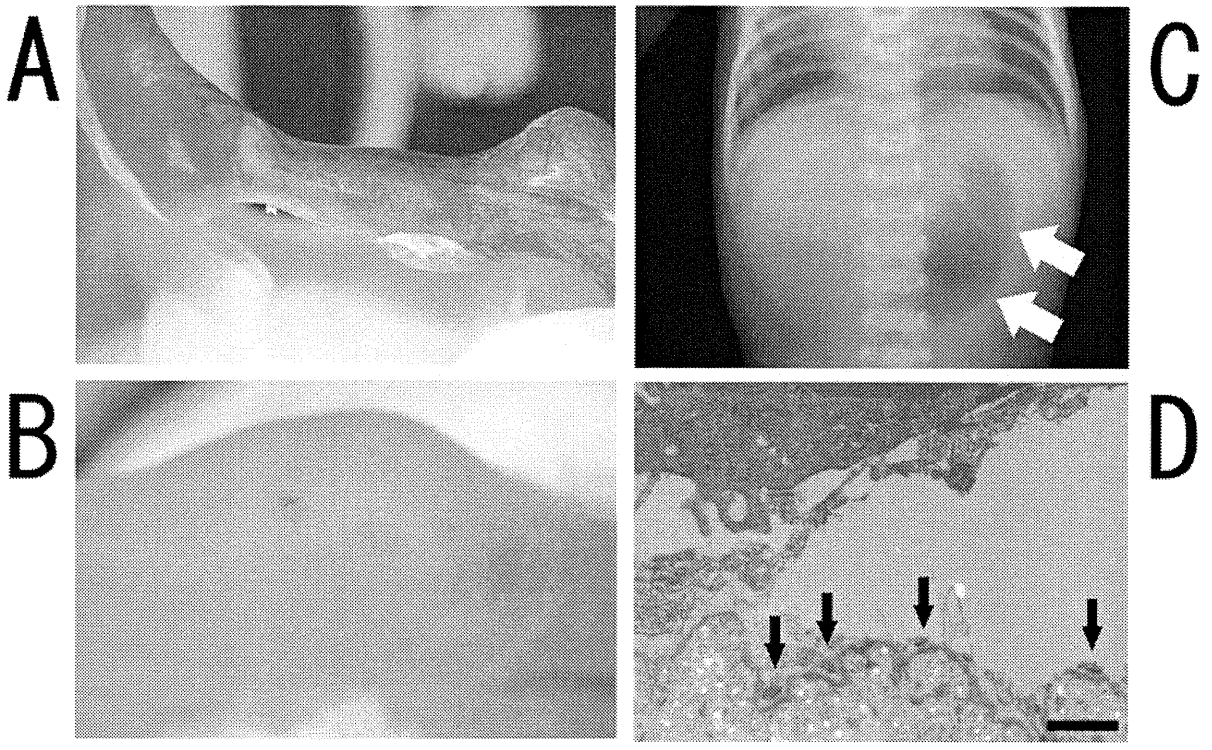

Figure 2. Clinical and ultrastructural features of the proband. (A) Aplasia cutis is observed on the left lower leg at birth. (B) Vesicles and erosions are scattered on the right knee. (C) Abdominal X-ray reveal single bubble sign (arrows), which indicated pyloric atresia. (D) Electron microscopy of the skin specimens from the proband reveals skin detachment within basal keratinocytes. Hemidesmosomes are hypoplastic and are observed at the base of the blisters (arrows) (Bar=1μm).

PLEC Mutations in Exon 32

PLEC mutational analysis demonstrated that the proband was compound heterozygous for maternal c.10984C>T (p.Glu3662X) and de novo c.11453_11462del in exon 32, the last exon of *PLEC* (Fig. 3A, 3B, 1C). The latter mutation is predicted to result in a frameshift that causes 88-amino-acid missense sequences followed by a premature termination codon (PTC). Both of the mutations were novel. c.10984C>T was confirmed by *BsrI* restriction enzyme digestion (Fig. 3C). c.11453_11462del was also confirmed by *BbvCI* restriction enzyme digestion (Fig. 3D) and TA-cloning (data not shown). Haplotype analysis of this family using microsatellite markers excluded false paternity as well as false maternity (data not shown) to establish the de novo nature of c.11453_11463del. The father's sperm has not been tested, although it might be beneficial to exclude the small possibility of paternal germ-line mosaicism through analyzing the father's sperm for any future prenatal diagnosis. In addition, c.7587G>A (p. =) transition in exon 32 was also detected in one allele of the proband and his father. This c.7587G>A transition was found in 3 of 100 normal unrelated alleles (50 healthy Japanese individuals), and was likely a polymorphism.